Proc. Natl. Acad. Sci. USA
Vol. 88, pp. 11037–11041, December 1991
Neurobiology

Magnetic field tomography of coherent thalamocortical 40-Hz oscillations in humans

(Alzheimer disease/magnetic resonance imaging/cognition/auditory activity)

U. RIBARY*, A. A. IOANNIDES†, K. D. SINGH†, R. HASSON†, J. P. R. BOLTON†, F. LADO*, A. MOGILNER*, AND R. LLINÁS*‡

*Center for Neuromagnetism, Department of Physiology and Biophysics, New York University Medical Center, New York, NY 10016; and †Department of Physics, The Open University, Milton Keynes, MK7 6AA, United Kingdom

Contributed by R. Llinás, July 30, 1991

ABSTRACT **This paper introduces the use of magnetic field tomography (MFT), a noninvasive technique based on distributed source analysis of magnetoencephalography data, which makes possible the three-dimensional reconstruction of dynamic brain activity in humans. MFT has a temporal resolution better than 1 msec and a spatial accuracy of 2–5 mm at the cortical level, which deteriorates to 1–3 cm at depths of 6 cm or more. MFT is used here to visualize the origin of a spatiotemporally organized pattern of coherent 40-Hz electrical activity. This coherence, initially observed during auditory input, was proposed to be generated by recurrent corticothalamic oscillation. In support of this hypothesis, we illustrate well-defined 40-Hz coherence between cortical–subcortical sites with a time shift that is consistent with thalamocortical conduction times. Studies on Alzheimer patients indicate that, while a similar activity pattern is present, the cortical component is reduced in these subjects.**

In the past decade significant advances have been made in noninvasive technology capable of imaging brain activity with sufficient spatial resolution to complement the structural imaging analysis offered by magnetic resonance imaging (MRI) (1) and computerized tomography (2). However, all imaging techniques available to date fall short of the optimal temporal resolution.

The utilization of electrical or magnetic signals has been known to afford the necessary temporal resolution but, until very recently, magnetoencephalography (MEG) analysis was based solely on the assumption of a single point source, the current dipole (3–7), which is only valid when the underlying activity is highly localized and, in general, cannot support imaging capabilities. The development of inverse problem algorithms with primary sources specified by continuous current densities confined to a well-defined region referred to as the source space (8–10) removes the limitations of point source models in the spatial domain without imposing restrictions on the temporal resolution. In earlier work, some of us used a two-dimensional surface as the source space (8, 9). In this paper, we solve the inverse problem by using a three-dimensional source space (a cylinder). This three-dimensional solution allows the generation of a set of two-dimensional images that provide a sequence of slices through the source space. Each image shows the square of the magnitude of the current density at points in the appropriate slice, represented by a color map ranging from black (low activity) to yellow (high activity). By analogy with computerized tomography and positron emission tomography (11), we call this technique magnetic field tomography (MFT). The basic methodology utilized here has been extensively tested and the results have shown excellent reproducibility with computer-generated data (refs. 8 and 9; see Fig. 1*C*). The two-dimensional paradigm was initially tested on spontaneous and evoked activity in normal subjects and in patients (8, 12).

We describe here, as an example of the applicability of MFT, the three-dimensional organization of a newly discovered thalamocortical 40-Hz oscillation in human subjects. Oscillatory activity in the 40-Hz range has been observed in humans and in many other mammalian species (13–19) and has been reported to be generated during cognitive tasks (13). It has been extensively studied at New York University Medical Center by using a variety of experimental paradigms (20–22).

A 14-channel MEG system (Biomagnetic Technologies) was used. It consists of a magnetically shielded room, two cryogenic Dewar flasks with seven magnetic sensors each, and a probe position indicator to determine position and orientation of the sensors with respect to the head (5). Magnetic 40-Hz activity was recorded over an entire cerebral hemisphere, using several paradigms (see *Results*).

METHODS

We have developed an imaging system based on a probabilistic formulation of the biomagnetic inverse problem (8, 9). The main features of this system are outlined below. The measured flux m_i at the ith detector is taken to be a linear function of the primary current density $\mathbf{j}(\mathbf{r})$:

$$m_i = \int \mathbf{j}(\mathbf{r}) \cdot \mathbf{f}_i(\mathbf{r}) d^3r.$$

The vector function $\mathbf{f}_i(\mathbf{r})$ is the lead field of the ith detector and can be interpreted as its sensitivity profile. The (x, y, z) components of $\mathbf{f}_i(\mathbf{r})$ are proportional to the signals generated at the ith detector by primary unit dipoles located at $\mathbf{r}$ and aligned with the (x, y, z) coordinate axes.

To obtain a solution to the biomagnetic inverse problem, we choose a source space S (a region of space within which the primary currents are presumed to be confined), a probability weight function $w(\mathbf{r})$ (which gives an *a priori* probability distribution for the primary current density within S), and a regularization parameter ζ (which stabilizes the inversion of a nearly singular system of equation). A detailed mathematical analysis that maximizes the probabilistic entropy of the primary current density then shows that the expectation value $\mathbf{j}(\mathbf{r})$ of the primary current density can be

The publication costs of this article were defrayed in part by page charge payment. This article must therefore be hereby marked "*advertisement*" in accordance with 18 U.S.C. §1734 solely to indicate this fact.

Abbreviations: MFT, magnetic field tomography; MRI, magnetic resonance imaging; MEG, magnetoencephalography.

‡To whom reprint requests should be addressed at: Department of Physiology and Biophysics, New York University Medical Center, 550 First Avenue, New York, NY 10016.

expressed as a weighted linear combination of the lead field functions

$$\mathbf{j}(\mathbf{r}) = \sum_{k=1}^{n} a_k \mathbf{f}_k(\mathbf{r}) w(\mathbf{r}),$$

where the coefficients a_k are related to the measurements m_i by the linear system

$$\sum_{k=1}^{n} P_{ik} m_k = \sum_{k,j=1}^{n} (P_{ij} P_{jk} + \zeta P_{ik}) a_k,$$

and the matrix element P_{ik} is the overlap of the scalar product of the ith and kth lead fields over the source space weighted by $w(\mathbf{r})$. The regularization parameter is chosen according to principles discussed previously (8, 9); a suitable choice makes the method robust to noise by ensuring that unreasonably large current densities are excluded from the solution. If the a priori probability weight function $w(\mathbf{r})$ were taken to be uniform, the method would automatically favor superficial sources. To compensate for this, we have chosen a weight function that increases with depth in such a way that the depths of trial current dipoles are correctly reproduced. Fig. 1*C* displays examples of the degree of spatial resolution for a set of computer-generated data concerning two current dipoles at different depths. Such trial inversions provide a most severe test for the method because of the continuity properties of the lead field functions. An iterative schema reduces the spread of the solutions but in general it does not eliminate it completely. With an appropriately chosen a priori probability weight, the maximum MFT solution coincides closely with the position of single or double dipoles (deep or superficial) that generated the signals—e.g., Fig. 1*C*. Earlier studies with computer-generated data (8, 9) have shown that localized regions of activity can be identified with accuracies comparable to those obtained by current dipole inversion algorithms and, more importantly, that it is possible to reproduce the form of intricate extended current distributions that are resistant to current dipole modeling.

To analyze the corticothalamic oscillations, we chose our source space to be a cylinder (radius, 4.5 cm; depth, 4 cm); the most superficial face of the cylinder, which faced the sensor array, was oriented over the temporal, inferior frontal, and inferior parietal cortices around the auditory cortex. The deep face of the cylinder contained deeper structures such as thalamus and basal ganglia (Fig. 2). This choice of source space was influenced by the geometry of magnetic recordings and restricted only the primary current density. To facilitate the display of our solutions, we use a set of nine tomographic disks, each 0.5 cm apart, obtained by taking slices through the cylindrical source space at right angles to its main axis. The square of the current density modulus was displayed within each circular slice as a set of MFT images (Fig. 2). In cases where the variation of activity with depth was to be emphasized, the intensity was averaged within each slice before being displayed (Fig. 3).

A relative color scale was used for displaying the MFT solutions; the scale is linear with color sequence, from almost no activity to maximal or saturating activity (1.0): black < green < red < yellow.

Oscillatory magnetic fields alternating in time with a positive–negative polarity result in a MFT solution with time alternating polarity. Because current density is a vector valued function, a scalar quantity, the square of the current density, is represented instead in the images of electrical brain activity. The squaring of the current density over time produces an apparent frequency doubling, as shown in Figs. 3 and 4. Such frequency doubling arises through filtering procedures when the MEG recording baseline is set to the mean, or DC value, of an oscillatory signal. This results in a signal that oscillates between positive and negative extrema, instead of a signal that oscillates between zero and a positive extremum or between zero and a negative extremum only.

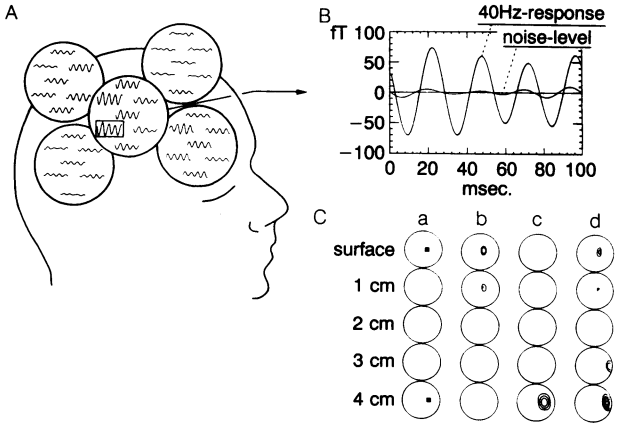

FIG. 1. Probe locations and magnetic steady-state auditory responses in a healthy human. (*A*) Recording positions over the right hemisphere. (*B*) Averaged (500 epochs) 40-Hz response and averaged (500 epochs) noise level of the system for a given representative channel (within box in *A*). (*C*) MFT inversions obtained from trial data generated by point sources (current dipoles); the true locations of current dipoles are indicated by solid squares in column a. The geometric arrangement (including source space, conducting sphere, and detectors) is identical to that used in MFT analysis of experimental data. Columns b–d show the three-dimensional MFT solution in a series of five slices, 1 cm apart, through a cylindrical source space. Each slice contains a contour plot of the square of the expectation value of the current density. The same a priori probability weight was used in three reconstructions from signals with a moderate amount of noise. Columns: b, a unit current dipole at the top of the cylinder, c, a current dipole of strength 5 units at the bottom of the cylinder; d, both current dipoles in b and c. For signals generated by a single current dipole, the position of the target source coincided with the maximum of the MFT solution for both the superficial (column b) and deep dipoles (column c). When both dipoles are active (column d), the deepest source is displaced from its true position.

The spatial resolution of MFT images decreases with depth at a rate that depends on the specific details of the experimental arrangement—e.g., sensor type, head coverage, and sensor spacing as well as the noise in the data. There is additional distortion at deeper levels since the contribution from primary sources at the center of a conducting sphere is zero. The solution must, therefore, be carefully interpreted in the deeper layers of the cylinder. However, since the human head is not exactly spherical, nonzero contributions from deep generators will appear in the solutions at approximately the right depth, but they will be somewhat displaced from the center. The presence or absence of activity within deeper layers of the cylinder can be reliably detected and distinguished from activity at the cortical level as demonstrated by the inversions of computer-generated data in Fig. 1*C*. In this connection, note also that our inversions of real data produce regions of high activity at consistent and reproducible depths (Fig. 3), in spite of the fact that our solutions are generated independently from one moment to the next.

RESULTS AND DISCUSSION

Recently, 40-Hz activity has been recorded in carnivores. This activity was restricted to localized brain areas or to small cell groups such as a few cortical columns (18). Moreover, the results were taken to indicate the local, sensory-specific temporal coordination of activity in cortical neurons whose coherence was based on an intracortical mechanism (18). We thought, however, that the 40-Hz oscillatory activity ob-

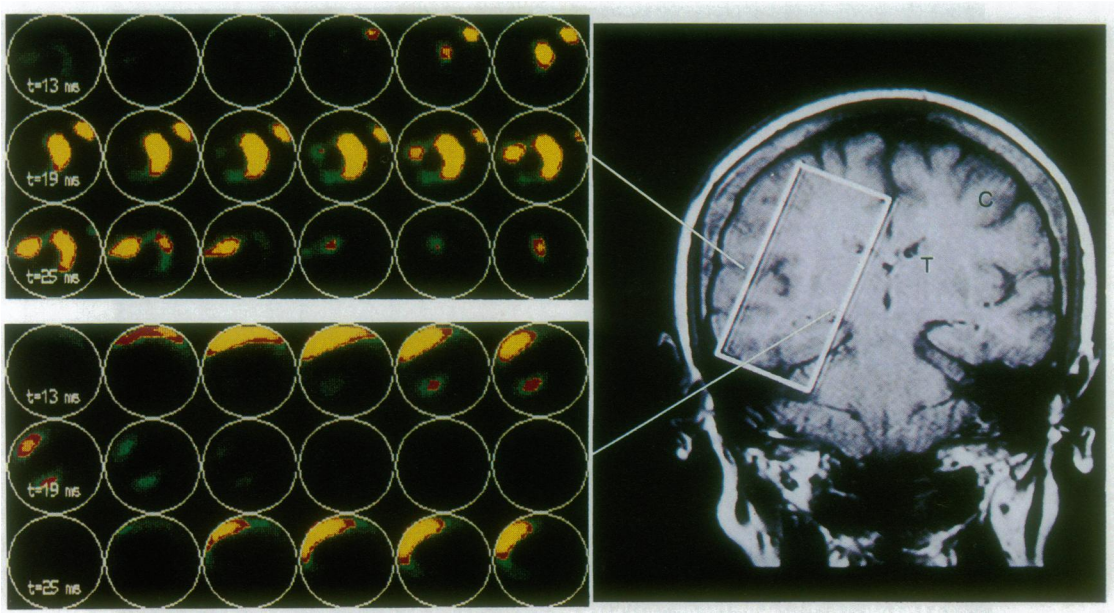

FIG. 2. The evolution of MFT images of 40-Hz activity recorded from a normal elderly adult over time at the cortical level (*Upper Left*) and the thalamic level (*Lower Left*). The location of the cylindrical source space is outlined on the coronal MRI scan (*Right*). (The cylinder is viewed from the side and so appears as a rectangle.) The top face of the cylinder is close to the temporal area around the auditory cortex (c), while the bottom face is close to the thalamus (T). The axis of the cylinder was the midpoint of the symmetrical MEG-probe placement. In the color MFT images (*Left*) the cylinder, viewed from above, appears as a disk with a circular boundary. The MFT solutions (each represented by a separate circle) are shown every millisecond from 13 to 30 msec within an averaged epoch of 100 msec of the steady-state 40-Hz response such that the rostral portion of the brain corresponds to the right edge of each circle and the caudal portion corresponds to the left edge. Note that the activity is initiated in the rostral part of the subcortical slice and seems to rotate to the caudal and ventral regions. Three milliseconds later, the cortical activity is observed rostrally and the main sensory area (center) is activated accompanied by an activity that rotates and terminates at the caudal pole of the cylinder. Note also that the pattern recurs every 12.5 msec (corresponding to 0.5 cycle of a 40-Hz sine wave). It is clear that the onset of activity at the thalamic level precedes the onset of activity at the cortical level by ≈3 msec. This sequence of activity appears to progress in an organized fashion over various depths within the volume of the thalamocortical systems (see also Fig. 3).

served in various brain areas reflected a common global mechanism (20) and have hypothesized the involvement of thalamocortical pathways in the organization of this event (23). This hypothesis is supported by the experimental results and MFT analysis presented in this paper.

Magnetic 40-Hz oscillatory activities were recorded from 30–35 positions over the right hemisphere (Fig. 1 *A* and *B*) and analyzed at 1-msec steps. The data were obtained from 15 individuals; 5 normal young adults, 5 patients with severe dementia, and 5 normal elderly adults matched for age and sex with the patients (20). Magnetic 40-Hz activity was recorded during auditory processing elicited in the initial tasks by steady-state 40-Hz auditory stimulation (20), a paradigm initially described by Galambos and coworkers (14), and in most cases by transient sound stimuli with random patterns and frequencies (22), the latter in order to avoid possible resonance with the stimulus. Using MFT and comparing both stimulus paradigms, we found that synchronized 40-Hz activity is a major oscillatory event during auditory processing. This 40-Hz activity was highly organized in three-dimensional space and in time and was independent of stimulus parameters, thus confirming previous findings (20, 22–24).

The MFT solutions are shown in Figs. 2 and 3. They support earlier suggestions that the 40-Hz activity is generated by recurrent thalamocortical activity (20, 22, 23, 25) and is not restricted to single areas (14, 26). In particular, the MFT results show a large electrical coherence that is spatially and temporally organized and occurs as an alternation of superficial and deeper activity; an onset of activity at the thalamic level is followed by widespread activation of the thalamocortical system, which results in coherent thalamocortical oscillations. This oscillatory process has a frequency near 40 Hz (Fig. 3), is absent from higher or lower frequency bands, and displays an organized continuous rostral–caudal phase shift.

These findings indicate the presence of phase-locked magnetic 40-Hz oscillations over large cortical areas (Fig. 2) and confirm other recent findings (22). MEG recordings revealed that the 40-Hz oscillatory activity during auditory processing had the following properties: (*i*) it was recorded over the entire hemisphere, (*ii*) it was independent of the stimulus presentation rate, (*iii*) it was clearly phase-locked over cortical areas [as measured within the area of one probe (25 cm^2)] for periods of 100–200 msec relative to the start of stimulus presentation (22). Moreover, a phase shift of oscillatory activity with an apparent motion from the frontal to the occipital pole of the head has been reported during auditory processing (22). In earlier studies, the magnetic field pattern of this 40-Hz oscillatory activity over the head surface was found to be highly organized in space and time and was suggested to reflect a complex, time-locked sequence of network function, with a focus on the activated sensory area (20). In particular, a stereotyped temporal pattern of magnetic activity was found. It consisted of a positive–negative field sequence that rotated in a continuous phase shift over the frontal, temporal, parietal, and occipital areas (20). In addition, MEG recordings consistently found large phase differences of synchronized 40-Hz activity over the entire hemisphere during auditory processing (22). There was a small but clear phase shift among the seven sensors within one cryogenic Dewar flask, which could be followed as a continuous event over distance along the entire hemisphere. This continuous phase shift of oscillatory activity was within a prime frequency band near 40 Hz, occurred from the frontal to the occipital pole of the hemisphere, and corresponded to a rostral–caudal shift of 4–6 msec (22, 24). This phase shift has been proposed to be due to a wave of coherent 40-Hz

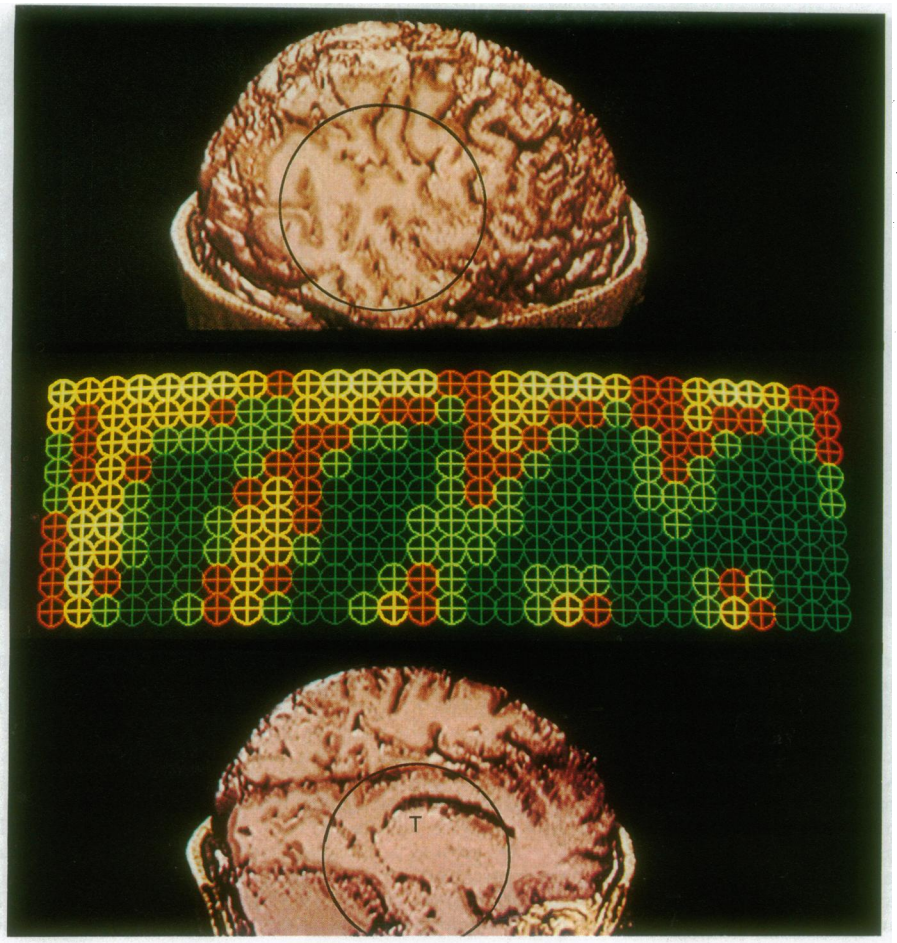

FIG. 3. MFT solutions for the transient 40-Hz activity in a normal adult (31 years old) during auditory processing (*Middle*) (analyzed within the frequency band of 35–45 Hz). (*Top* and *Bottom*) The cylinder is face-on (dark circle on the three-dimensional subject). (*Bottom*) The level of the deepest disk (thalamic level). (*Top*) The level of the most superficial disk within the cylindrical source space (cortical level). (*Middle*) Serial evolution of the average activity progresses from the thalamic to the cortical level, through each of the nine disks (0.5 cm apart) within the three-dimensional cylindrical source space and over time, and at time steps of 1.95 msec. The abscissa represents the time, which increases to the right, while depth is represented by the ordinate (superficial levels are shown above the deeper levels). Serial activity is shown from 61 to 116 msec after the onset of the stimulus presentation. A clear and large coherence within thalamocortical systems is seen near 40 Hz.

electrical activity sweeping along the cortex each 12.5 msec (22). Preliminary data obtained using a 37-channel MEG system (Biomagnetic Technologies) (which has a lower noise level and improved sensor equipment than the 14-channel system) indicates that similar sweep-like activity can be observed in nonaveraged, single epochs before as well as during auditory processing. This indicates that 40-Hz activity is continually generated by the central nervous system and can be best observed and averaged when reset and enhanced by sensory input.

In a second set of studies, the temporal and spatial organization of these oscillations was found to be modified in patients with Alzheimer disease (20, 27). Indeed, 40-Hz activity within thalamocortical systems was altered in these patients (Fig. 4). Although the rhythmic pattern was clearly seen in this patient, as well as the time lag between activity in the cortical and thalamic levels, the intensity of the rhythm was reduced and the waveform was deteriorated, particularly at the cortical level. These changes were typical of the Alzheimer patients studied. Since one of the common pathological indicators of Alzheimer disease is neuronal degeneration, especially of dendrites, with a concomitant decrease in cortical volume and an increase in ventricular space, the decrease of the magnetic signal at the cortical level is consistent with this pathology (28, 29). Changes in the shape of the waveform may reflect a deterioration of the feedback resonance between the cortex and thalamus (22). However, further investigation is necessary to demonstrate the detailed spatial and temporal alterations of the 40-Hz response and how they are correlated to the pathology of the disease.

The latter results, as well as those obtained in normal individuals, support the hypothesis that recurrent thalamic–cortical–thalamic activity is involved in organizing and maintaining coherent 40-Hz activity. Moreover, the size and global distribution of the 40-Hz coherent response suggests that it is a major mechanism of brain function representing a spatially and temporally organized synchronization of cortical activity reinforced by corticothalamic pathways having as a focus the activated sensory area. This is particularly attractive given the recent findings from intracellular studies in cortical interneurons (25) and thalamic cells (30). As for the hypothesis of a scanning-like process, more detailed data analysis is necessary.

In conclusion, MFT is a noninvasive methodology that allows the imaging of dynamic brain function in three dimensions with high temporal resolution (Figs. 2–4). The utilization of this approach in the study of cognitive function in normal and pathologic conditions opens a significant window for the clinical world. We propose that the presence of a coherent sweep of thalamocortical resonance at 40 Hz and its alteration in pathological conditions such as Alzheimer disease may reflect a functional scanning of brain activity (22). This scanning may serve as a temporal conjunctive structure responsible for amalgamating multiple sensory components into a single cognitive event.

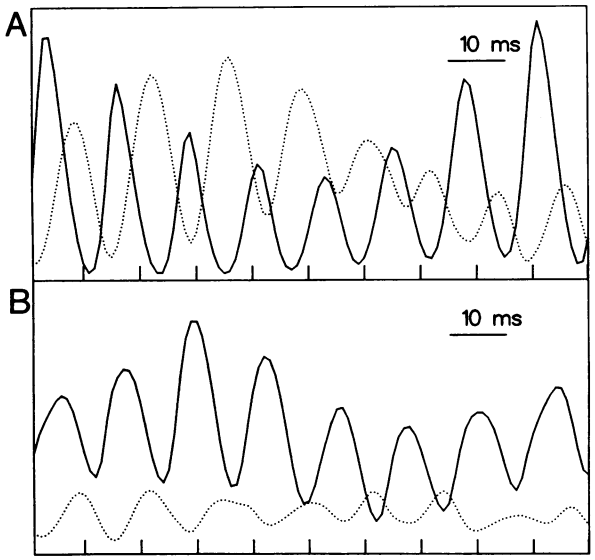

FIG. 4. Activation curves representing the average current density from two slices within the cylindrical source space. The average current density from the most superficial disk (cortical level; dotted line) and the average current density of the deepest disk (thalamic level; solid line) are plotted against time in each frame. The variation of integrated activity is shown over a 100-msec period of an averaged epoch of the steady-state 40-Hz response for an elderly normal adult (74 years old) (*A*), and for an Alzheimer patient (71 years old) (*B*). The two traces in each frame are normalized with the peak current density magnitude in that time segment, so that activation of a particular disk varied between 0 and 1 (or 0% and 100%). Therefore, the two frames (*A* and *B*) do not show absolute but relative differences in the distribution of activation between the two subjects. Note that, as illustrated by these two examples, a comparison of the MFT images in normal subjects and in Alzheimer patients shows that the sharpness of the resonance is reduced in patients, particularly at the cortical level, indicating a smaller amplitude.

The authors wish to acknowledge the excellent technical support provided by Richard Jagow. Drs. S. Ferris and A. Kluger are thanked for referring patients from the Department of Psychiatry at New York University Medical Center. We further thank Drs. M. deLeon and G. Smith for the magnetic resonance image and Dr. H. Rusinek of the Department of Radiology for his contribution to the reconstruction of the three-dimensional MRI. The continuing support of Biomagnetic Technologies is gratefully acknowledged. The development of the MFT imaging system has benefited from Science and Engineering Research Council (U.K.) support under the Computational Science Initiative, and the collaboration between New York University and the Open University has been promoted by the provision of Open University and Nuffield Foundation travel grants to A.A.I.

1. Wehrli, F. W., Shaw, D. & Kneeland, J. B. (1988) *Biomedical Magnetic Resonance Imaging: Principles, Methodology and Applications* (VCH, New York).
2. Brooks, R. A. & diChiro, G. (1976) *Phys. Med. Biol.* **21**, 689–732.
3. Williamson, S. J. & Kaufman, L. (1981) *J. Magn. Mater.* **22**, 129–201.
4. Hari, R. & Ilmoniemi, R. J. (1986) *Biomed. Eng.* **14**, 93–126.
5. Yamamoto, T., Williamson, S., Kaufman, L., Nicholson, C. & Llinas, R. (1988) *Proc. Natl. Acad. Sci. USA* **85**, 8732–8736.
6. Nomura, M., Ribary, U., Lopez, L., Mogilner, A., Lado, F. & Llinas, R. (1990) *Soc. Neurosci. Abstr.* **16**, 702.
7. Suk, J., Ribary, U., Cappell, J., Yamamoto, T. & Llinas, R. (1991) *Electroencephalogr. Clin. Neurophysiol.* **78**, 185–196.
8. Ioannides, A. A., Bolton, J. P. R., Hasson, R. & Clarke, C. J. S. (1989) in *Advances in Biomagnetism*, eds. Williamson, S., Hoke, M., Stroink, G. & Kotani, M. (Plenum, New York), pp. 591–594.
9. Ioannides, A. A., Bolton, J. P. R. & Clarke, C. J. S. (1990) *Inverse Probl.* **6**, 523–542.
10. Clarke, C. J. S. & Janday, B. S. (1989) *Inverse Probl.* **5**, 483–500.
11. Hoffman, E. J. & Phelps, M. E. (1986) in *Positron Emission Tomography and Autoradiography: Principles and Applications for the Brain and the Heart*, ed. Phelps, M. E. (Raven, New York), pp. 237–286.
12. Ioannides, A. A., Hasson, R. & Miseldine, G. J. (1990) *Proc. SPIE Int. Soc. Opt. Eng.* **1351**, 471–481.
13. Sheer, D. E. (1989) in *Brain Dynamics*, eds. Basar, E. & Bullock, T. H. (Springer, Berlin), pp. 339–374.
14. Galambos, R., Makeig, S. & Talmachoff, P. J. (1981) *Proc. Natl. Acad. Sci. USA* **78**, 2643–2647.
15. Bouyer, J. J., Montaron, M. F., Vahnee, J. M., Albert, M. P. & Rougeul, A. (1987) *Neuroscience* **22**, 863–869.
16. Bressler, S. L. & Freeman, W. J. (1980) *Electroencephalogr. Clin. Neurophysiol.* **50**, 19–24.
17. Eckhorn, R., Bauer, R., Jordan, W., Brosch, M., Kruse, W., Munk, M. & Reitboeck, H. J. (1988) *Biol. Cybern.* **60**, 121–130.
18. Gray, C. M. & Singer, W. (1989) *Proc. Natl. Acad. Sci. USA* **86**, 1698–1702.
19. Von der Malsburg, C. (1986) in *Brain Theory*, eds. Palm, G. & Aertsen, A. (Springer, Berlin), pp. 161–176.
20. Ribary, U., Llinas, R., Kluger, A., Suk, J. & Ferris, S. H. (1989) in *Advances in Biomagnetism*, eds. Williamson, S., Hoke, M., Stroink, G. & Kotani, M. (Plenum, New York), pp. 311–314.
21. Ribary, U. & Llinas, R. (1990) *Eur. J. Neurosci. Suppl.* **3**, 51 (abstr.).
22. Llinas, R. & Ribary, U. (1991) in *Induced Rhythms in the Brain*, eds. Basar, E. & Bullock, T. (Birkhaeuser, Boston), Chapter 7, in press.
23. Llinas, R. (1990) *Fidia Res. Found. Symp. Ser.* **4**, 173–192.
24. Ribary, U., Weinberg, H., Cheyne, D., Johnson, B., Holliday, S. & Ancill, R. J. (1988) *Eur. J. Neurosci. Suppl.* **1**, 44.17.
25. Llinas, R., Grace, A. A. & Yarom, Y. (1991) *Proc. Natl. Acad. Sci. USA* **88**, 897–901.
26. Maekelae, J. P. & Hari, R. (1987) *Electroencephalogr. Clin. Neurophysiol.* **66**, 539–546.
27. Ribary, U., Llinas, R., Kluger, A., Cappell, J., Suk, J. & Ferris, S. H. (1990) *Electroencephalogr. Clin. Neurophysiol.* **75**, S126.
28. Scheibel, A. B., Wechsler, A. F. & Brazier, M. A. B. (1986) *Biological Substrates of Alzheimer's Disease* (Academic, New York).
29. Damasio, A. R. & Hoesen, G. W. (1986) in *Biological Substrates of Alzheimer's Disease*, eds. Scheibel, A. B., Wechsler, A. F. & Brazier, M. A. B. (Academic, New York), pp. 65–71.
30. Steriade, M., Curro Dossi, R., Pare, D. & Oakson, G. (1991) *Proc. Natl. Acad. Sci. USA* **88**, 4396–4400.